

Lateral competition for cortical space by layer-specific horizontal circuits

Hillel Adesnik¹ & Massimo Scanziani¹

The cerebral cortex constructs a coherent representation of the world by integrating distinct features of the sensory environment. Although these features are processed vertically across cortical layers, horizontal projections interconnecting neighbouring cortical domains allow these features to be processed in a context-dependent manner. Despite the wealth of physiological and psychophysical studies addressing the function of horizontal projections, how they coordinate activity among cortical domains remains poorly understood. We addressed this question by selectively activating horizontal projection neurons in mouse somatosensory cortex, and determined how the resulting spatial pattern of excitation and inhibition affects cortical activity. We found that horizontal projections suppress superficial layers while simultaneously activating deeper cortical output layers. This layer-specific modulation does not result from a spatial separation of excitation and inhibition, but from a layer-specific ratio between these two opposing conductances. Through this mechanism, cortical domains exploit horizontal projections to compete for cortical space.

The axons of pyramidal cells in layer 2/3 project vertically, across layers, and expand horizontally, within layers, to contact neighbouring cortical domains (for example, orientation domains in visual cortex or whisker representation domains in somatosensory cortex)^{1–7}. Layer 2/3 pyramidal cells are thus poised to coordinate the activity of neighbouring domains with respect to their own⁸. The relationship between the spatial extents of excitation and inhibition generated by layer 2/3 pyramidal cells is likely to be instrumental in how these neurons regulate activity across and within layers. On one hand, the spatial extent of excitation generated by layer 2/3 pyramidal cells across and within layers can be inferred from anatomical and physiological data^{1–4,9,10}. On the other hand, the spatial extent of inhibition generated by layer 2/3 pyramidal cells through the recruitment of cortical inhibitory interneurons is harder to predict owing to the complexity and diversity of inhibitory axonal projections which can span multiple layers and extend horizontally over large cortical regions^{10–15}. Understanding how layer 2/3 pyramidal cells have an impact on the activity of neighbouring domains with respect to their own would reveal one of the key mechanisms coordinating cortical activity in space. To address this question we sought a stimulus that would selectively activate layer 2/3 in a manner that mimics physiological activity. Because of the pronounced gamma modulation that layer 2/3 neurons experience spontaneously¹⁶ or in response to sensory stimulation^{17–19}, we developed a protocol to induce gamma oscillations specifically in layer 2/3. This enabled us to avoid non-selectively driving activity in all layers of cortex by a sensory stimulus and therefore to study specifically the impact of layer 2/3 output in coordinating activity across and within cortical layers.

Photoinduced gamma oscillations

We expressed channelrhodopsin 2 (ChR2)^{20–22} in layer 2/3 pyramidal cells of the neocortex by *in utero* electroporation²³. Cortical expression of ChR2 was restricted to layer 2/3 excitatory neurons where $23 \pm 2\%$ ($n = 6$ slices) of pyramidal cells expressed the protein, consistent with previous observations^{24,25} (Fig. 1a and Supplementary Fig. 1a, b). Electroporated mice were anaesthetized and a small craniotomy was

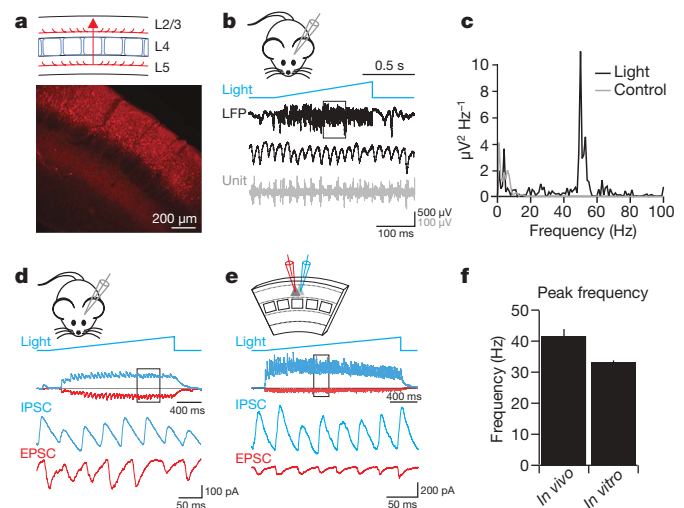


Figure 1 | Photoinduced gamma activity *in vivo* and *in vitro*. **a**, The top panel shows a schematic of a layer 2/3 pyramidal cell axon. The bottom panel shows anti-GFP immunostaining of the barrel cortex expressing ChR2 and GFP. **b**, A light ramp (blue, 1-s duration) induced oscillations of the local field potential (LFP, high-pass filtered at 0.5 Hz; top trace, black) and of unit activity (bottom trace, grey; LFP high-pass filtered at 100 Hz) recorded in layer 2/3 *in vivo*. The LFP in the grey box is expanded below. **c**, LFP power spectrum shown in **b** before (grey) and during (black) the light stimulus. **d**, *In vivo* recording of a layer 2/3 pyramidal cell during light stimulation. Top traces: red, excitation recorded at -70 mV. Blue, inhibition recorded at $+10$ mV. Baseline holding current has been subtracted. Bottom traces: expanded section of the traces in the grey box. **e**, Simultaneous recording of two layer 2/3 pyramidal cells *in vitro* during light stimulation. Top traces: red, excitation recorded at -70 mV in one cell; blue, inhibition recorded at $+10$ mV simultaneously in the other cell. Bottom traces: expanded section of traces in the grey box. **f**, Average peak frequency between 20 and 60 Hz (\pm s.e.m.) of the light-induced oscillations recorded *in vivo* ($n = 16$) and *in vitro* ($n = 65$; $P = 0.004$).

¹Howard Hughes Medical Institute, Center for Neural Circuits and Behavior, Neurobiology Section and Department of Neurosciences, University of California San Diego, La Jolla, California 92093-0634, USA.

performed to expose the Chr2-expressing somatosensory cortex. We stimulated the exposed region with a long (2 s) ramp of blue light, that is, a photostimulus of gradually increasing intensity (see Methods); we used a ramp rather than a square pulse to avoid the fast desensitizing transient of the photocurrent²⁰ (Supplementary Fig. 1c) and monitored population activity with an extracellular electrode inserted in layer 2/3. Notably, rather than triggering a flurry of uncoordinated neuronal activity, photostimulation generated rhythmic oscillation of the local field potential (LFP) at gamma frequency (average 42 ± 2 Hz, $n = 16$; Fig. 1b, c) that was accompanied by the activity of simultaneously recorded units, spiking in phase with the LFP (Fig. 1b). The power of the photoinduced oscillation was 2,000-fold ($\pm 1,200$, $n = 16$, $P = 0.02$) larger than the power at the same frequency in the unstimulated cortex (Fig. 1c). The oscillation persisted as long as the photostimulus was on and could be reliably and repeatedly evoked. Furthermore, the oscillation frequency increased only a little ($\sim 25\%$) with the intensity of the photostimulus (Supplementary Fig. 2). Importantly, neither the rhythmic activity per se nor the specific frequency of the oscillation was imposed by the photostimulus²⁶, because apart from its onset, offset and progressive increment in intensity, the photostimulus was devoid of any temporal structure. Thus, stimulation of pyramidal cells in layer 2/3 of the neocortex *in vivo* initiates self-organized oscillations within the gamma frequency range.

Consistent with naturally occurring gamma oscillations, photostimulation initiated rhythmic activity of both inhibitory and excitatory postsynaptic currents (IPSCs and EPSCs, respectively)^{16,27,28} in layer 2/3 neurons recorded *in vivo* in the whole-cell configuration (average amplitude of individual cycles: EPSCs, 169 ± 76 pA; IPSCs, 777 ± 228 pA; $n = 4$, Fig. 1d). To avoid contamination of synaptic conductances by direct Chr2-mediated photocurrents, we only considered whole-cell recordings from neurons not expressing Chr2 (Supplementary Fig. 3).

Photoinitiated gamma activity could also be induced in cortical slices *in vitro* (Fig. 1e). Photostimulation induced robust oscillations of the EPSCs and IPSCs recorded simultaneously from pairs of layer 2/3 pyramidal cells (33 ± 1 Hz, $n = 6$; Fig. 1e). The rhythmic activity relied on both glutamatergic and GABAergic transmission, as it was abolished by application of either the glutamate receptor antagonists NBQX (2,3-dioxo-6-nitro-1,2,3,4-tetrahydrobenzo[f]quinoxaline-7-sulphonamide) and CPP (3-((R)-2-carboxypiperazin-4-yl)-propyl-1-phosphonic acid) (5 and 10 μ M, $n = 8$), or the GABA_A (γ -aminobutyric acid subtype A) receptor antagonist gabazine (400 nM, $n = 11$; a subsaturating concentration was chosen to avoid epileptiform activity; Supplementary Fig. 4). Similar oscillations could also be induced in other neocortical regions expressing Chr2 in layer 2/3 pyramidal cells such as visual cortex (28 ± 1 Hz; $n = 12$) or cingulate cortex (26 ± 1 Hz; $n = 10$). These data show that expression of Chr2 in layer 2/3 neocortical pyramidal cells permits reliable initiation of self-organizing rhythmic activity within the gamma frequency band both *in vivo* and *in vitro*. With this technique we can now determine the spatial extent of excitation and inhibition generated by activity of layer 2/3 pyramidal cells vertically, across layers, and horizontally, within layers, and establish the resulting impact on the activity of neighbouring cortical domains.

Vertical match of excitation and inhibition

Activity in layer 2/3 could generate three distinct vertical patterns of inhibition relative to excitation: inhibition could be (1) more broadly distributed across layers than excitation; (2) complementary to excitation such that layers that receive less excitation receive more inhibition; or (3) restricted to the same layers receiving excitation. We performed *in vitro* recordings from principal neurons in several cortical layers of the somatosensory cortex simultaneously while initiating oscillatory activity in layer 2/3 with light stimulation. Figure 2a illustrates a simultaneous voltage-clamp recording from four principal neurons located in each of layers 2/3, 4, 5 and 6. Voltage clamping the neurons at the IPSC reversal potential to isolate EPSCs shows

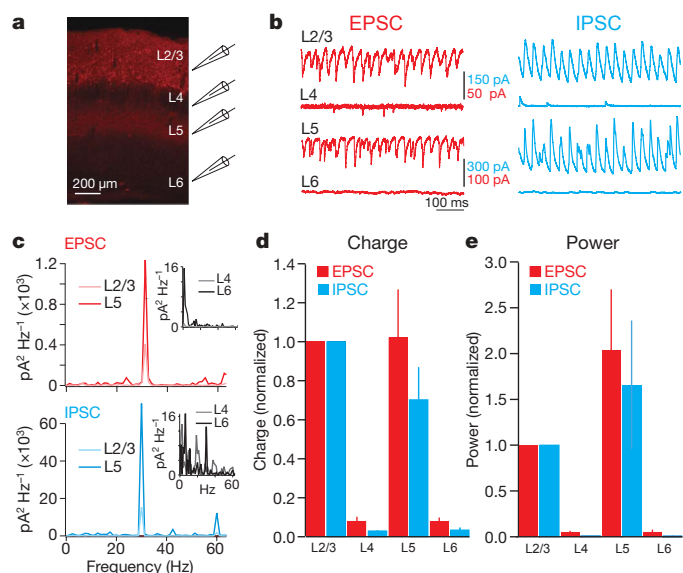


Figure 2 | Vertical match of excitation and inhibition across layers.

a, Recording configuration. **b**, EPSCs (left) and IPSCs (right) recorded simultaneously in L2/3, L4, L5 and L6 principal cells. **c**, Power spectra of the EPSCs (top) and IPSCs (bottom) for currents recorded in layer 2/3 and layer 5 pyramidal cells (from **b**). Insets show power spectra for layer 4 and 6 neurons; the y axis of the insets is expanded as compared to the main y axis. **d**, Average normalized charge (\pm s.e.m.) for simultaneously recorded cells across cortical layers. In each recording, one of the cells was a layer 2/3 pyramidal cell for normalization (EPSC charge, $P < 10^{-6}$: L2/3 ($n = 58$), L4 ($n = 16$), L5 ($n = 34$), L6 ($n = 15$); IPSC charge, $P < 10^{-7}$: L2/3 ($n = 53$), L4 ($n = 16$), L5 ($n = 32$), L6 ($n = 13$); one way ANOVA). **e**, Average normalized power (\pm s.e.m.) between 20–60 Hz for photoinduced oscillations across cortical layers (EPSC power, $P < 10^{-7}$: L2/3 ($n = 46$), L4 ($n = 15$), L5 ($n = 20$), L6 ($n = 14$); IPSC power, $P < 10^{-3}$: L2/3 ($n = 53$), L4 ($n = 15$), L5 ($n = 30$), L6 ($n = 13$); one way ANOVA).

that both synaptic excitatory charge and oscillatory power are maximal in layers 2/3 and 5 and minimal in layers 4 and 6 (Fig. 2b and Methods), consistent with anatomical and physiological observations^{1–4,9,10,29}. Notably, voltage clamping the same neurons at the EPSC reversal potential to isolate IPSCs revealed that inhibition was precisely confined to the same cortical layers receiving excitation (Fig. 2b). Because layer 5 in the somatosensory cortex consists of two sublayers (5A and 5B), the principal neurons of which have distinct functional properties³⁰, we compared the distribution of excitation and inhibition generated by activity in layer 2/3 between the two sublayers (Supplementary Fig. 5). Both sublayers received excitation and inhibition in response to activity in layer 2/3, yet layer 5A received significantly less of both conductances as compared to layer 5B ($P < 0.05$; Supplementary Fig. 5a–c and Methods). Taken together, these data demonstrate a remarkable overlap in the spatial domains of excitation and inhibition generated during activity in layer 2/3. The two opposed conductances are precisely confined to layer 5, the main cortical output layer, and layer 2/3, the main input to layer 5.

Horizontal match of excitation and inhibition

Next we determined the relative pattern of excitation and inhibition horizontally across domains within individual layers. Again, one could expect three different scenarios: inhibition extends over a larger area as compared to excitation, resulting in surround inhibition³¹; excitation extends over a larger area as compared to inhibition, resulting in surround excitation³²; or excitation and inhibition cover matching areas³³. For these experiments, we restricted photostimulation to a circular zone of $\sim 90 \mu\text{m}$ in diameter centred on layer 2/3 above a barrel (see Methods). The spatial extent of neuronal recruitment by this circular photostimulus was approximately one barrel column in diameter (see Methods and Supplementary Fig. 6a).

Light ramps induced oscillations at gamma frequency, indicating that even the photostimulation of a restricted area of layer 2/3 is sufficient to initiate rhythmic activity (Fig. 3). Notably, this oscillation was generated by pyramidal cells whose somatodendritic compartment was localized within the photostimulated area, because bypassing axons expressing ChR2 do not contribute to oscillatory activity (Supplementary Fig. 6b).

We recorded from layer 2/3 or layer 5 pyramidal cells and initiated oscillations in each of four barrel columns located on both sides of the barrel column within which the pyramidal cells were recorded. The oscillation propagated horizontally at an average speed of $240 \pm 50 \text{ mm s}^{-1}$ ($n = 6$; see Methods), consistent with the propagation speed of cortical waves³⁴ and the conduction velocity in cortical axons^{35,36}. Both synaptic excitatory charge and oscillation power decayed with increasing distance from the site it had originated from (excitatory charge and power decayed to $26 \pm 4\%$ and $26 \pm 6\%$ ($n = 18$, charge, $P = 0.002$; power, $P = 4 \times 10^{-7}$) in layer 2/3 and to $37 \pm 8\%$ and $30 \pm 8\%$ in layer 5 when oscillations were initiated two barrel columns away ($n = 12$); Fig. 3b, c). Notably, the decay of synaptic inhibitory charge and oscillatory power was nearly identical with the decay of excitation (inhibitory charge and power decayed to $23 \pm 5\%$ and $26 \pm 8\%$ ($n = 18$), respectively, in layer 2/3 and to $27 \pm 7\%$ and $23 \pm 12\%$ in layer 5 when oscillations were initiated two barrel columns away ($n = 12$, charge, $P = 2 \times 10^{-7}$; power, $P = 0.001$; Fig. 3b, c)). Thus, despite their progressive decay with distance from the site the oscillation had originated from (Fig. 3b, c), the ratio between excitation and inhibition remained constant.

The horizontal decay of synaptic excitation and inhibition was region specific, in that synaptic excitation and inhibition fell much more sharply when oscillations were initiated in the adjacent non-barrel cortex compared to the parent barrel cortex (excitatory and inhibitory charge decayed to $9 \pm 1\%$ and $15 \pm 3\%$ ($n = 11$), respectively, when oscillations were initiated 400 μm away in the adjacent cortex, versus $28 \pm 2\%$ and $31 \pm 7\%$ ($n = 12$) in the parent barrel cortex; $P = 0.0004$ for excitation and 0.004 for inhibition; Fig. 3d).

Furthermore, the coronal plane of the slice did not have an impact on the horizontal extent of synaptic excitation and inhibition as slices cut tangentially to the surface of the somatosensory cortex showed comparable spatial decays (see Methods and Supplementary Fig. 7).

Taken together these results show a spatially delimited yet precisely overlapping distribution of excitation and inhibition vertically, across layers, and horizontally, within layers, across cortical domains.

Layer-specific modulation of activity

To understand the role of layer 2/3 pyramidal cells in coordinating cortical activity we addressed how the two spatially matched but opposing conductances affect neuronal spiking across and within layers.

We recorded from both layer 2/3 and 5 pyramidal cells in the current-clamp configuration and depolarized the neurons with 1-s-long current injections to trigger action potentials (average rate $6.4 \pm 0.7 \text{ Hz}$, $n = 31$, range 2–12 Hz; Fig. 4a) to allow us to monitor bidirectional changes in firing rates. Photoinduced oscillatory activity invariably and significantly suppressed the spike rate of layer 2/3 pyramidal cells ($84 \pm 5\%$ reduction, $n = 11$, $P = 1.5 \times 10^{-5}$; Fig. 4a, b). In striking contrast, the spike rate of layer 5 pyramidal cells was significantly facilitated ($170 \pm 20\%$ increase, $n = 20$, $P = 0.037$; Fig. 4a, b). Spiking in layer 2/3 pyramidal cells was invariably suppressed up to two barrel columns away from the initiation site of the oscillation (Fig. 4c). The suppression was most pronounced within the home barrel column ($85 \pm 7\%$ reduction, $n = 8$, $P = 0.004$) and progressively decreased with increasing horizontal distance ($28 \pm 8\%$ decrease two barrel columns away, $n = 8$, $P = 7 \times 10^{-5}$; Fig. 4c). In contrast, the spike rate of layer 5 pyramidal cells was significantly facilitated up to two barrel columns away from the initiation site of the oscillation, an effect that was again most pronounced within the home barrel column ($100 \pm 19\%$ increase, $n = 6$, $P = 10^{-5}$) and decreased progressively with increasing horizontal distance ($10 \pm 10\%$ increase two columns away, $P = 0.02$; Fig. 4c). Pyramidal cells in both sublayers 5A and 5B were facilitated, and this facilitation occurred over a similar horizontal distance from the initiation site of

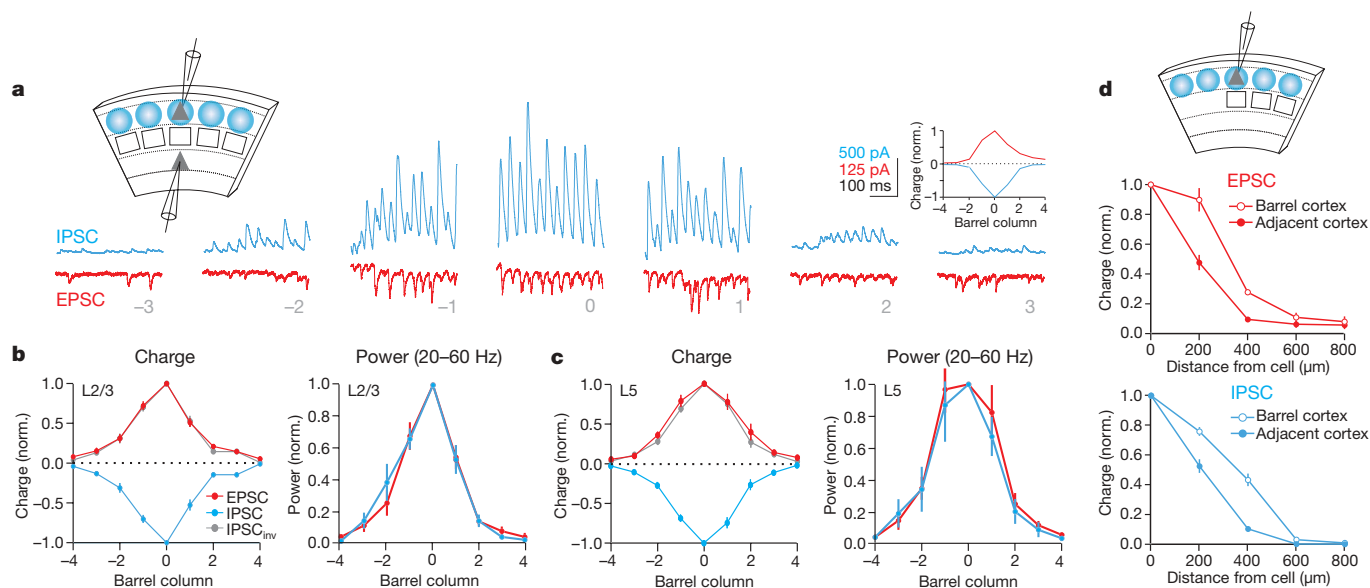


Figure 3 | Horizontal match of excitation and inhibition within layers. **a**, The recording configuration is shown at the top left. Blue and red traces indicate IPSCs and EPSCs, respectively, recorded in a layer 2/3 pyramidal cell in response to focal light stimulation translated tangentially across barrel columns. Numbers below traces indicate distance (in barrel columns) of the light-stimulated barrel column with respect to the home barrel column (position 0). The inset to the right shows normalized charge (excitation in red and inhibition in blue) plotted against distance. **b**, Plots of average charge (left) and power between 20–60 Hz (right) against distance in layer

2/3 pyramidal cells ($n = 19$). **c**, Same as **b** but for layer 5 pyramidal cells ($n = 12$). **d**, Top panel: recording configuration at the edge of barrel cortex. Middle and bottom panels: average charge plotted against distance (in micrometres) between the recorded neuron and the centre of light stimulus when the stimulus was on barrel cortex (open circles) or on adjacent somatosensory non-barrel cortex (closed circles). Red indicates excitation ($n = 10$); blue indicates inhibition ($n = 10$). In all plots error bars are \pm s.e.m.

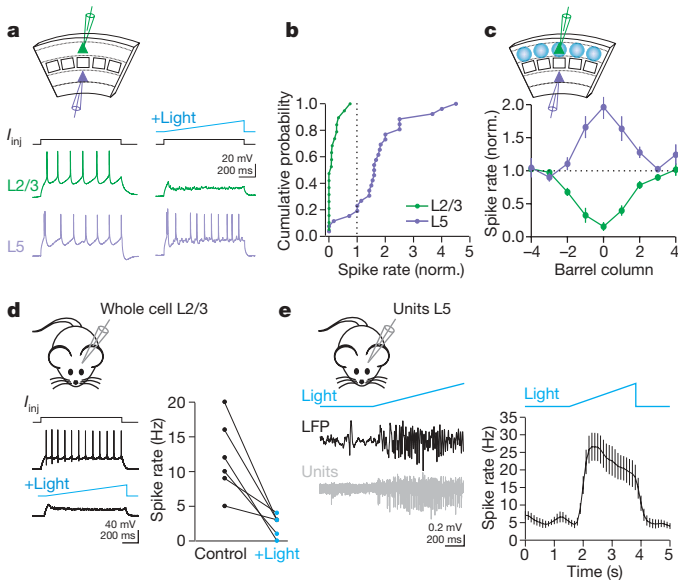


Figure 4 | Lateral suppression and feed-forward facilitation *in vivo* and *in vitro*. **a**, Response of simultaneously recorded layer 2/3 (green) and layer 5 (purple) pyramidal cells to current injection (I_{inj}) without (left) and with (right) light stimulation. **b**, Cumulative probability plot of the normalized spike rate (spike rate with light stimulus divided by the spike rate in control: layer 2/3, green ($n = 11$); layer 5, purple ($n = 20$); $P < 0.001$, Kolmogorov–Smirnov test). **c**, Normalized spike rate of layer 2/3 (green, $n = 8$) and layer 5 (purple, $n = 6$) pyramidal cells plotted against barrel-column distance from focal light stimulation. Error bars are \pm s.e.m. **d**, The left panel shows *in vivo* response of layer 2/3 neuron to current injection (I_{inj}) without (top) and with (bottom, digitally subtracted bridge) light stimulation. The right panel shows a summary plot ($n = 6$). **e**, The left panel shows LFP (top trace, black, high-pass filtered at 1 Hz) and unit activity (bottom trace, grey; LFP high-pass filtered at 300 Hz) recorded in layer 5 *in vivo* in response to light stimulation. The right panel shows average time course of spike rate of seven similar experiments. Error bars are \pm s.e.m.

the oscillation (Supplementary Fig. 5f). These results show that activity in layer 2/3 generates lateral suppression of spiking in layer 2/3 pyramidal cells and feed-forward facilitation of layer 5 pyramidal cells. The horizontal pattern of suppression in layer 2/3 is mirrored by the horizontal pattern of facilitation in layer 5 (Fig. 4c). Thus, layer 2/3 pyramidal cells can efficiently drive downstream layer 5 pyramidal cells lying both directly below as well as in neighbouring domains, while simultaneously suppressing the main input to layer 5 by inhibiting neighbouring layer 2/3 pyramidal cells.

The same opposed modulation of layer 2/3 and 5 excitability also occurred *in vivo*. Layer 2/3 neurons were recorded in the whole-cell configuration to ensure the absence of ChR2 expression and prevent direct photostimulation. Multiunit activity was recorded in layer 5 with extracellular electrodes. Photoinitiated oscillations significantly suppressed spiking of layer 2/3 neurons ($73 \pm 8\%$ decrease, $n = 5$, $P = 0.003$; Fig. 4d) but strongly increased spiking in layer 5 ($600 \pm 200\%$ increase, $n = 7$, $P = 0.0004$; Fig. 4e). These data indicate that oscillations in layer 2/3 pyramidal cells have an impact on their home and neighbouring domains in a layer-specific manner, generating suppression of layer 2/3 and facilitation of layer 5.

Layer-specific excitation/inhibition ratio

What mechanism accounts for the opposite modulation of layer 2/3 and layer 5 pyramidal cells? Simultaneous recordings (Fig. 5a) showed that the average excitatory charge recorded from the soma of pyramidal cells was not significantly different between layer 2/3 and layer 5 pyramidal cells (107 ± 11 pC versus 108 ± 14 pC, $n = 34$ pairs, $P = 0.97$; for comparison between layer 5A and 5B pyramidal cells see Supplementary Fig. 5c–e). In contrast, the inhibitory charge recorded at the soma was significantly smaller in layer 5 pyramidal

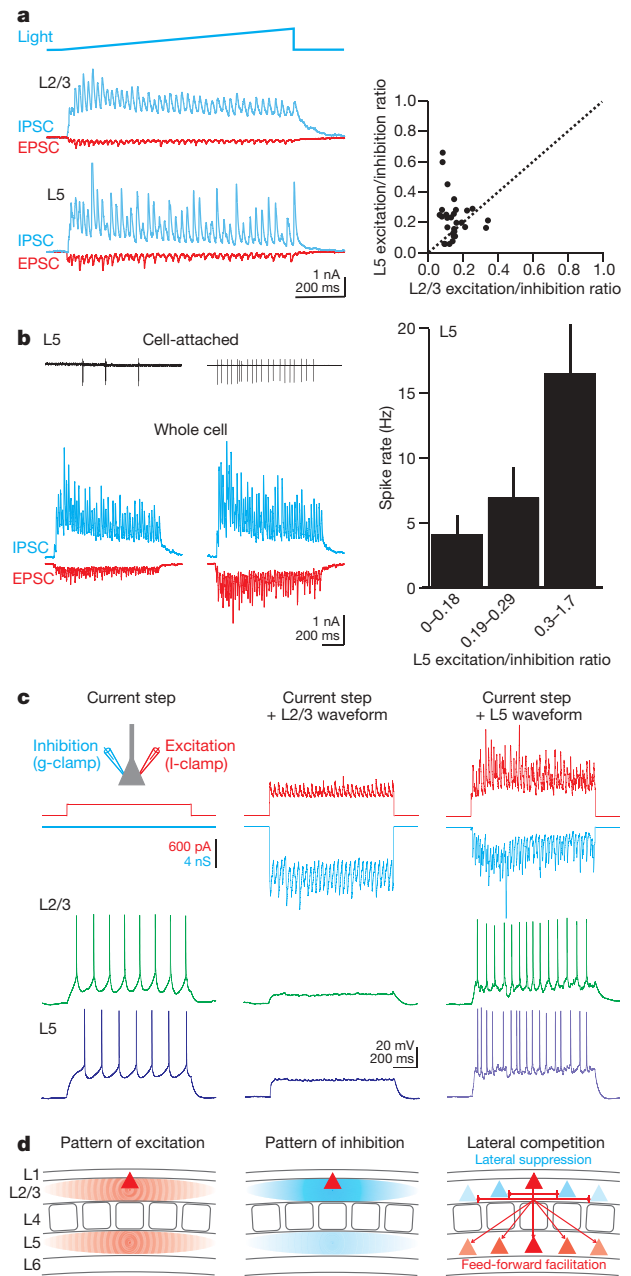


Figure 5 | Layer-specific excitation/inhibition ratio. **a**, The left panel shows simultaneous recording of layer 2/3 (top) and layer 5 (bottom) pyramidal cells during light stimulation (EPSCs in red and IPSCs in blue). The right panel shows scatter plot of excitation/inhibition ratio for all layer 2/3 and layer 5 cell pairs ($n = 30$; $P = 0.018$). **b**, The left panel shows cell-attached (top) and subsequent whole-cell recordings (bottom) from a pair of layer 5 pyramidal cells during light stimulation. The right panel shows binned distribution of spike rate versus excitation/inhibition ratio for 35 layer 5 pyramidal cells (the bins contain, from left to right: 12, 12 and 11 pairs). Error bars are \pm s.e.m. **c**, The top panel shows recording configuration and injected waveforms. One pipette imposes an inhibitory conductance (blue; g-clamp). The other pipette injects an excitatory current waveform (red, I-clamp). The left panel shows the square depolarizing current step used to elicit baseline spiking; no inhibitory conductance. Middle and right panels show inhibitory conductance (blue) and excitatory current (red) waveforms, recorded in a layer 2/3 pyramidal cell (middle) and in a layer 5 pyramidal cell (right). The bottom panel shows response of a layer 2/3 (green) and a layer 5 (purple) pyramidal cell to the current step and waveforms illustrated above. **d**, Schematic of the spatial overlap between excitation (left) and inhibition (centre) across and within layers. The resulting lateral suppression within layer 2/3 and feed-forward excitation of layer 5 leads to the lateral expansion of a cortical domain at the expense of its neighbours (right).

cells ($24 \pm 10\%$ smaller; 780 ± 70 pC versus 570 ± 70 pC, $n = 30$ pairs, $P = 0.029$). More importantly, however, the ratio between somatic excitation and inhibition across simultaneously recorded pairs was substantially larger in layer 5 pyramidal cells ($120 \pm 40\%$ larger; excitation/inhibition ratio L5, 0.26 ± 0.04 ; L2/3, 0.15 ± 0.02 , $n = 30$ pairs, $P = 0.018$; Fig. 5a), indicating the possibility that differences in somatic excitation/inhibition ratio may, at least in part, account for the facilitation of layer 5 pyramidal cells. Consistent with this possibility, we found that the spiking probability of individual layer 5 pyramidal cells (determined in the cell-attached mode during light-induced oscillations) increased with larger excitation/inhibition ratios (determined subsequently in the whole-cell configuration; Fig. 5b, one-way analysis of variance (ANOVA), $P = 0.047$).

To establish directly whether the layer-specific difference in somatic excitation/inhibition ratio underlies lateral suppression in layer 2/3 versus feed-forward facilitation in layer 5 we replayed synaptic waveforms recorded from layer 2/3 into layer 5 pyramidal cells and vice versa (Fig. 5c). Specifically, the soma of pyramidal cells was patched with two pipettes, one to inject the excitatory current and the other to dynamically clamp the inhibitory conductance (the chosen waveforms were representative of the average somatic excitation/inhibition ratio; see Methods). The playback of waveforms recorded in a layer 2/3 pyramidal cell into the soma of layer 5 pyramidal cells completely suppressed their firing ($100 \pm 0\%$ reduction, $n = 6$, $P = 0.006$; the same was true when the waveform was played back into L2/3 pyramidal cells, $100 \pm 0\%$ reduction, $n = 6$, $P = 10^{-5}$; Fig. 5c). In contrast, playback of waveforms recorded in a layer 5 pyramidal cell into the soma of layer 2/3 pyramidal cells strongly facilitated their firing (L2/3, $120 \pm 20\%$ increase, $n = 6$, $P = 0.025$; the same occurred when the waveforms were played back into layer 5 pyramidal cells, $120 \pm 10\%$ increase, $n = 6$, $P = 0.015$).

Thus, these results demonstrate that layer-specific differences in the excitation/inhibition ratio can account for the lateral suppression of layer 2/3 and feed-forward facilitation of layer 5 pyramidal cells.

Discussion

Physiological and psychophysical studies suggest that horizontal interactions between cortical domains enable information to be processed in a context-dependent manner^{3,8,37–42}. By selectively activating neurons that generate horizontal projections we revealed a layer-specific coordination of cortical activity. Horizontal projections originating from layer 2/3 pyramidal cells suppress layer 2/3 while facilitating layer 5. This layer-specific modulation extends over several domains around the activated population of layer 2/3 pyramidal cells, indicating that active layer 2/3 pyramidal cells can drive layer 5 pyramidal cells within their own and neighbouring domains while suppressing neighbouring layer 2/3 pyramidal cells. It should be noted that not only is layer 2/3 the main input to layer 5 but that layer 5 gives rise to the main cortical output. Thus, layer 2/3 horizontal projections can drive the output of neighbouring domains (by activating layer 5) while silencing the inputs to these neighbouring outputs (by suppressing layer 2/3). This coordinated modulation of superficial and deep layers generates competition between neighbouring domains and may allow the representation of one domain to expand dynamically at the cost of its neighbours (Fig. 5d).

Within the rodent's somatosensory cortex, the density of horizontal axons diminishes with increasing distance (over hundreds of micrometres) between barrel columns³. In other systems, in addition to a local decrease in the density of horizontal projections, long-range (millimetres) projections preferentially link cortical domains with similar response characteristics^{5–7}. Future studies will establish whether layer-specific modulation also holds true for long-range interactions.

We show that the layer-specific facilitation and suppression is achieved by differences in excitation/inhibition ratio, rather than by spatially separating these two opposing conductances. Furthermore, we show that despite their progressive decrease in amplitude within

layers, the ratio of these two conductances remains constant. These data thus highlight the distinct roles of ratio and amplitude of the two conductances on spike rate modulation: whereas the ratio determines the sign of the effect (that is, whether facilitating or suppressing) the amplitude determines its magnitude.

The specific inhibitory circuits activated here will have to be elucidated in the future. It is possible that different inhibitory circuits may be recruited by distinct activity patterns (for example, different oscillation frequencies), resulting in different spatial and amplitude relationships between excitation and inhibition. This possibility is supported by frequency-dependent routing of inhibition⁴³.

Taken together, our data illustrate a simple scheme by which axons of layer 2/3 pyramidal cells coordinate excitation and inhibition to promote competition for cortical space between neighbouring cortical domains.

METHODS SUMMARY

For *in utero* electroporation²³ E15–E16 embryos were injected with 1–2 μ g ChR2 DNA and 0.5–1 μ g of GFP or mRFP DNA. Somatosensory thalamocortical slices⁴⁴ were cut and stored in reduced sodium artificial cerebrospinal fluid (ACSF) before being transferred 1–4 h later to a submerged temperature-controlled recording chamber in standard ACSF. Whole-cell recordings were obtained with patch pipettes (2–3 M Ω) containing a caesium-based internal solution for voltage-clamp experiments, and a potassium-based solution for current-clamp recordings. For *in vivo* recordings mice were anaesthetized with 1% isoflurane and 1.25 mg kg⁻¹ chlorprothixene, their head fixed and a small (~ 2 –2.5 mm) craniotomy performed. The dura mater was left intact for extracellular recordings, or a small incision was made to permit the entry of patch pipettes for whole-cell recordings. For photostimulation a mounted 5W blue LED was used, collimated and coupled to the epifluorescence path of an Olympus BX51 through a 40 \times water immersion lens. For *in vivo* photostimulation a 3W LED was coupled to a 1-mm diameter optic fibre and mounted < 5 mm from the craniotomy. Intracellular and LFP data were recorded using Multiclamp 700B or 200B amplifiers, and digitized at 10–20 kHz (National Instruments), while multichannel recording was conducted with an AM systems 16 channel amplifier and digitized at 30 kHz. For replay of synaptic currents, L2/3 and L5 pyramidal cells were patched with two pipettes; one pipette injected the excitatory waveform, the other imposed an inhibitory conductance using a custom feedback-controlled analogue 'dynamic clamp' circuit board.

Full Methods and any associated references are available in the online version of the paper at www.nature.com/nature.

Received 6 November 2009; accepted 11 February 2010.

- Binzegger, T., Douglas, R. J. & Martin, K. A. A quantitative map of the circuit of cat primary visual cortex. *J. Neurosci.* **24**, 8441–8453 (2004).
- Gottlieb, J. P. & Keller, A. Intrinsic circuitry and physiological properties of pyramidal neurons in rat barrel cortex. *Exp. Brain Res.* **115**, 47–60 (1997).
- Petersen, C. C., Grinvald, A. & Sakmann, B. Spatiotemporal dynamics of sensory responses in layer 2/3 of rat barrel cortex measured *in vivo* by voltage-sensitive dye imaging combined with whole-cell voltage recordings and neuron reconstructions. *J. Neurosci.* **23**, 1298–1309 (2003).
- Feldmeyer, D., Lubke, J. & Sakmann, B. Efficacy and connectivity of intracolumnar pairs of layer 2/3 pyramidal cells in the barrel cortex of juvenile rats. *J. Physiol. (Lond.)* **575**, 583–602 (2006).
- Bosking, W. H., Zhang, Y., Schofield, B. & Fitzpatrick, D. Orientation selectivity and the arrangement of horizontal connections in tree shrew striate cortex. *J. Neurosci.* **17**, 2112–2127 (1997).
- Gilbert, C. D. & Wiesel, T. N. Columnar specificity of intrinsic horizontal and corticocortical connections in cat visual cortex. *J. Neurosci.* **9**, 2432–2442 (1989).
- Malach, R., Amir, Y., Harel, M. & Grinvald, A. Relationship between intrinsic connections and functional architecture revealed by optical imaging and *in vivo* targeted biocytin injections in primate striate cortex. *Proc. Natl Acad. Sci. USA* **90**, 10469–10473 (1993).
- Gilbert, C. D. & Wiesel, T. N. The influence of contextual stimuli on the orientation selectivity of cells in primary visual cortex of the cat. *Vision Res.* **30**, 1689–1701 (1990).
- Lefort, S., Tomm, C., Floyd Sarria, J. C. & Petersen, C. C. The excitatory neuronal network of the C2 barrel column in mouse primary somatosensory cortex. *Neuron* **61**, 301–316 (2009).
- Thomson, A. M., West, D. C., Wang, Y. & Bannister, A. P. Synaptic connections and small circuits involving excitatory and inhibitory neurons in layers 2–5 of adult rat and cat neocortex: triple intracellular recordings and biocytin labelling *in vitro*. *Cereb. Cortex* **12**, 936–953 (2002).

11. Ascoli, G. A. *et al.* Petilla terminology: nomenclature of features of GABAergic interneurons of the cerebral cortex. *Nature Rev. Neurosci.* **9**, 557–568 (2008).
12. Helmstaedter, M., Sakmann, B. & Feldmeyer, D. Neuronal correlates of local, lateral, and translaminar inhibition with reference to cortical columns. *Cereb. Cortex* **19**, 926–937 (2009).
13. Gupta, A., Wang, Y. & Markram, H. Organizing principles for a diversity of GABAergic interneurons and synapses in the neocortex. *Science* **287**, 273–278 (2000).
14. Kawaguchi, Y. & Kubota, Y. GABAergic cell subtypes and their synaptic connections in rat frontal cortex. *Cereb. Cortex* **7**, 476–486 (1997).
15. Fukuda, T., Kosaka, T., Singer, W. & Galuske, R. A. Gap junctions among dendrites of cortical GABAergic neurons establish a dense and widespread intercolumnar network. *J. Neurosci.* **26**, 3434–3443 (2006).
16. Hasenstaub, A. *et al.* Inhibitory postsynaptic potentials carry synchronized frequency information in active cortical networks. *Neuron* **47**, 423–435 (2005).
17. Gray, C. M., König, P., Engel, A. K. & Singer, W. Oscillatory responses in cat visual cortex exhibit inter-columnar synchronization which reflects global stimulus properties. *Nature* **338**, 334–337 (1989).
18. Nase, G., Singer, W., Monyer, H. & Engel, A. K. Features of neuronal synchrony in mouse visual cortex. *J. Neurophysiol.* **90**, 1115–1123 (2003).
19. Jones, M. S. & Barth, D. S. Sensory-evoked high-frequency (gamma-band) oscillating potentials in somatosensory cortex of the unanesthetized rat. *Brain Res.* **768**, 167–176 (1997).
20. Nagel, G. *et al.* Channelrhodopsin-2, a directly light-gated cation-selective membrane channel. *Proc. Natl Acad. Sci. USA* **100**, 13940–13945 (2003).
21. Li, X. *et al.* Fast noninvasive activation and inhibition of neural and network activity by vertebrate rhodopsin and green algae channelrhodopsin. *Proc. Natl Acad. Sci. USA* **102**, 17816–17821 (2005).
22. Boyden, E. S., Zhang, F., Bamberg, E., Nagel, G. & Deisseroth, K. Millisecond-timescale, genetically targeted optical control of neural activity. *Nature Neurosci.* **8**, 1263–1268 (2005).
23. Saito, T. & Nakatsuji, N. Efficient gene transfer into the embryonic mouse brain using *in vivo* electroporation. *Dev. Biol.* **240**, 237–246 (2001).
24. Petreanu, L., Huber, D., Sobczyk, A. & Svoboda, K. Channelrhodopsin-2-assisted circuit mapping of long-range callosal projections. *Nature Neurosci.* **10**, 663–668 (2007).
25. Pouille, F., Marin-Burgin, A., Adesnik, H., Atallah, B. V. & Scanziani, M. Input normalization by global feedforward inhibition expands cortical dynamic range. *Nature Neurosci.* **12**, 1577–1585 (2009).
26. Cardin, J. A. *et al.* Driving fast-spiking cells induces gamma rhythm and controls sensory responses. *Nature* **459**, 663–667 (2009).
27. Atallah, B. V. & Scanziani, M. Instantaneous modulation of gamma oscillation frequency by balancing excitation with inhibition. *Neuron* **62**, 566–577 (2009).
28. Bartos, M. *et al.* Fast synaptic inhibition promotes synchronized gamma oscillations in hippocampal interneuron networks. *Proc. Natl Acad. Sci. USA* **99**, 13222–13227 (2002).
29. Kampa, B. M., Letzkus, J. J. & Stuart, G. J. Cortical feed-forward networks for binding different streams of sensory information. *Nature Neurosci.* **9**, 1472–1473 (2006).
30. Manns, I. D., Sakmann, B. & Brecht, M. Sub- and suprathreshold receptive field properties of pyramidal neurones in layers 5A and 5B of rat somatosensory barrel cortex. *J. Physiol. (Lond.)* **556**, 601–622 (2004).
31. Douglas, R. & Martin, K. in *The Synaptic Organization of the Brain* (ed. Shepherd, G. M.) (Oxford Univ. Press, 1998).
32. Chance, F. S., Nelson, S. B. & Abbott, L. F. Complex cells as cortically amplified simple cells. *Nature Neurosci.* **2**, 277–282 (1999).
33. Anderson, J. S., Carandini, M. & Ferster, D. Orientation tuning of input conductance, excitation, and inhibition in cat primary visual cortex. *J. Neurophysiol.* **84**, 909–926 (2000).
34. Benucci, A., Frazor, R. A. & Carandini, M. Standing waves and traveling waves distinguish two circuits in visual cortex. *Neuron* **55**, 103–117 (2007).
35. Meeks, J. P. & Mennerick, S. Action potential initiation and propagation in CA3 pyramidal axons. *J. Neurophysiol.* **97**, 3460–3472 (2007).
36. Shu, Y., Duque, A., Yu, Y., Haider, B. & McCormick, D. A. Properties of action-potential initiation in neocortical pyramidal cells: evidence from whole cell axon recordings. *J. Neurophysiol.* **97**, 746–760 (2007).
37. Ramachandran, V. S. & Gregory, R. L. Perceptual filling in of artificially induced scotomas in human vision. *Nature* **350**, 699–702 (1991).
38. Hirsch, J. A. & Gilbert, C. D. Synaptic physiology of horizontal connections in the cat's visual cortex. *J. Neurosci.* **11**, 1800–1809 (1991).
39. Tucker, T. R. & Katz, L. C. Spatiotemporal patterns of excitation and inhibition evoked by the horizontal network in layer 2/3 of ferret visual cortex. *J. Neurophysiol.* **89**, 488–500 (2003).
40. Field, D. J., Hayes, A. & Hess, R. F. Contour integration by the human visual system: evidence for a local 'association field'. *Vision Res.* **33**, 173–193 (1993).
41. Shimegi, S., Ichikawa, T., Akasaki, T. & Sato, H. Temporal characteristics of response integration evoked by multiple whisker stimulations in the barrel cortex of rats. *J. Neurosci.* **19**, 10164–10175 (1999).
42. Mountcastle, V. B. & Powell, T. P. Neural mechanisms subserving cutaneous sensibility, with special reference to the role of afferent inhibition in sensory perception and discrimination. *Bull. Johns Hopkins Hosp.* **105**, 201–232 (1959).
43. Pouille, F. & Scanziani, M. Routing of spike series by dynamic circuits in the hippocampus. *Nature* **429**, 717–723 (2004).
44. Agmon, A. & Connors, B. W. Thalamocortical responses of mouse somatosensory (barrel) cortex *in vitro*. *Neuroscience* **41**, 365–379 (1991).

Supplementary Information is linked to the online version of the paper at www.nature.com/nature.

Acknowledgements We thank P. Abelkop for immunohistochemical labelling, J. Isaacson and R. Malinow for critical reading of the manuscript and the members of the Scanziani and Isaacson laboratory for advice during the course of the study. We thank K. Svoboda for pCAGGS-ChR2-Venus (Addgene 15753), C. Cepko for pCAG-GFP (Addgene 11150) and K. Deisseroth for sharing reagents. This work was supported in part by a grant from the National Institute for Mental Health (R01 MH70058). H.A. was supported by the Helen Hay Whitney Foundation. M.S. is an investigator of the Howard Hughes Medical Institute.

Author Contributions H.A. and M.S. designed the study. H.A. conducted all experiments and analysis. H.A. and M.S. wrote the paper.

Author Information Reprints and permissions information is available at www.nature.com/reprints. The authors declare no competing financial interests. Correspondence and requests for materials should be addressed to M.S. (massimo@ucsd.edu).

METHODS

In utero electroporation. Timed-pregnant ICR white mice (Charles River, E15–16) were anaesthetized with 2.5% isoflurane. The abdomen was cleaned with 70% ethanol and swabbed with iodine. A small vertical incision was made in the skin and abdominal wall and 8–12 embryos gently exposed. Each embryo was injected with 1–2 μ l of DNA solution and 0.05% Fast Green²³. pCAG-ChR2-Venus plasmid DNA was mixed with pCAG-GFP or pCAG-mRFP for a total of 1–2 μ g ChR2 DNA and 0.5–1 μ g of fluorophore DNA. We used a pressure-controlled bevelled glass pipette (Drummond, WPI Microbeveler) for injection. After each injection, the embryos were moistened with saline and voltage steps via tweezertrodes (BTX, 5 mm round, platinum, BTX electroporator) were applied at a zero degree angle with respect to the rostral–caudal axis of the head to target somatosensory cortex. To target cingulate cortex the polarity was reversed, and to target visual cortex the tweezertrodes were oriented 45° towards both the dorsal and caudal sides of the head. Voltage was 40 V for 5 pulses at 1 Hz, each pulse lasting 50 ms. The embryos were returned to the abdomen, which was sutured, followed by suturing of the skin. The procedure typically lasted under 20 min. On the day of birth animals were screened for location and strength of transfection by trans-cranial epifluorescence under an Olympus MVX10 fluorescence stereoscope.

Slice preparation. Cortical slices (400 μ m thick, unless stated otherwise) were prepared from the transfected hemispheres of mice aged P15–P40 using a DSK Microslicer in a reduced sodium solution containing (in mM) NaCl 83, KCl 2.5, MgSO₄ 3.3, NaH₂PO₄ 1, glucose 22, sucrose 72, CaCl₂ 0.5, and stored submerged at 34 °C for 30 min, then at room temperature for 1–4 h in the same solution before being transferred to a submerged recording chamber (Luigs and Neumann) maintained at 30–32 °C by inline heating in a solution containing (in mM) NaCl 119, KCl 2.5, MgSO₄ 1.3, NaH₂PO₄ 1.3, glucose 20, NaHCO₃ 26, CaCl₂ 2.5.

For radial slices from the somatosensory barrel cortex we used the thalamo-cortical plane⁴⁴; for slices from the visual or cingulate cortex we used the coronal plane; for tangential slices from the somatosensory cortex, the transfected hemisphere was trimmed on both the anterior and posterior side of barrel cortex with coronal cuts, placed on its anterior side and a cut was made with a scalpel so that much of barrel cortex lay in a plane parallel to cut. The surface of this last cut was glued to the slicer tray. The preparation was aided by the use of epifluorescent goggles to visualize the transfected area. Two to three 300–500 μ m slices were prepared, the first containing much of layer 2/3 and some of layer 4. In the slices containing layer 4, barrels could be identified under the microscope by transmitted light (Supplementary Fig. 7). Digital alignment of the images of the most superficial slices with the images of deeper slices containing most of layer 4 (using vasculature landmarks and the shape) allowed post-hoc identification of the photostimulated barrel columns.

Before the beginning of the recordings, all slices were inspected with epifluorescence to ascertain the location and quality of transfection.

To test for any age-dependent effects, we split our *in vitro* results into two groups, P14–21 (group 1) and P21–28 (group 2), containing nearly all our experiments. Excitation/inhibition ratio did not differ (0.17 ± 0.04 , $n = 25$ versus 0.16 ± 0.01 , $n = 24$, $P = 0.89$), nor did peak oscillation frequency (30 ± 1 Hz, $n = 34$ versus 30 ± 1 Hz, $n = 16$, $P = 0.95$), nor excitatory or inhibitory power (excitation (in $\text{pA}^2 \text{Hz}^{-1}$): $6.8 \times 10^4 \pm 8 \times 10^3$, $n = 34$ versus $9.8 \times 10^4 \pm 2.6 \times 10^4$, $n = 15$, $P = 0.24$; inhibition (in $\text{pA}^2 \text{Hz}^{-1}$): $3.7 \times 10^5 \pm 8 \times 10^4$, $n = 30$ versus $9 \times 10^5 \pm 3 \times 10^5$, $n = 15$, $P = 0.08$). However, net excitatory and inhibitory charge during the stimulus did increase with age (excitation: 51 ± 5 pC, $n = 30$ versus 125 ± 12 pC, $n = 29$, $P < 10^{-5}$; inhibition: 410 ± 44 pC, $n = 27$ versus 804 ± 72 pC, $n = 27$, $P < 10^{-4}$). As for evoked spiking, there were no differences in the per cent suppression of layer 2/3 ($75 \pm 13\%$, $n = 5$ versus $95 \pm 3\%$, $n = 6$, $P = 0.21$) or the per cent facilitation of layer 5 ($50 \pm 32\%$, $n = 10$ versus $90 \pm 50\%$, $n = 10$, $P = 0.52$). Thus, although apparent net synaptic input increases with age in response to the same light stimulus, all other features of the observed results are the same.

Recordings in vitro. Whole-cell recordings were obtained with pulled patch pipettes (2–3 M Ω) containing the following caesium-based internal solution (in mM): CsMeSO₄ 115, NaCl 8, HEPES 10, Na₃GTP 0.3, MgATP 4, EGTA 0.3, QX-314-Cl 5, tetraacesium BAPTA 10. For current-clamp recording, K-gluconate (140 mM) was substituted for CsMeSO₄, and QX-314 and BAPTA omitted. Voltage measurements were not corrected for the junction potential (8 mV established experimentally). Neurons were identified visually using oblique infrared videomicroscopy. Slices were placed in the recording chamber such that the top surface showed dendrites that were either parallel to the slice plane or such that the proximal portion of the apical dendrite was more superficial than the distal part. This ensured that recorded neurons had intact apical dendrites. Intactness of dendrites was confirmed in a subset of

recordings by visualization after inclusion of Alexafluor 568 in the internal solution. We routinely used epifluorescence to either avoid recordings from transfected neurons (as for most recordings), or to target them specifically. Series resistance (ranging from 6 to 20 M Ω) was not compensated, yet monitored continuously with negative voltage steps.

Recordings in vivo. Electroporated mice (average P44 \pm 21 (s.d.); $n = 18$) were anaesthetized with 2% isoflurane and 1.25 mg kg⁻¹ chlorprothixene and attached to a head post by dental acrylic. After removal of the scalp the transfected region was identified by epifluorescence and a small craniotomy (2–2.5 mm) drilled to expose the barrel cortex.

For extracellular recording the craniotomy was covered with 1% agarose and the dura left intact. A 16-channel linear silicon electrode array (NeuroNexus Technologies, model A16 (a1x16-3mm50-177)) was inserted at a $\sim 30^\circ$ angle with respect to the brain surface, 900–1,000 μ m into the cortex⁴⁵. The isoflurane was reduced to 1% and after 30 min data were collected for 1–2 h at 1–2 recording sites. The voltage signals were amplified (16 channel amplifier AM systems) and digitized at 30 kHz (Nidaq).

For whole-cell recordings a small incision was made in the dura and recordings established by standard blind patch techniques from neurons 150–400 μ m below the pia. Pipettes (2–3 M Ω) contained the caesium-based internal solution described above with the omission of QX-314 and BAPTA and the increase in CsMeSO₄ to 140 mM. Following giga-seal formation and break in cells were allowed 3–5 min to stabilize and dialyse before photostimulation was commenced. For voltage-clamp recordings access resistance was 21 ± 1 M Ω ($n = 5$). For *in vivo* current clamp recordings the K⁺ internal solution described above was used.

Photostimulation. For *in vitro* photostimulation a mounted 5 W blue LED (Thorlabs LEDC5) was collimated and coupled to the epifluorescence path of an Olympus BX51. All experiments were carried out under a 40 \times 0.8 NA water immersion lens.

For *in vivo* photostimulation a 1 mm optic fibre was coupled to a 3 W blue LED (Doric Lenses) and mounted <5 mm from the craniotomy.

Light intensity was controlled by the analogue output of an A/D card (NIDAQ, PCI6259) via a power supply (Thorlabs, LEDD1), and calibrated with photodiode and power meter. Light ramps had a duration of 1–2 s, a slope of 0.1–2.0 mW s⁻¹, started at zero intensity and reached a final intensity of 0.1–2.0 mW. The slope was adjusted for each slice to obtain a rhythmic activity with a largely stable power for the duration of the stimulus. Typically, the slope sufficient to trigger robust oscillations *in vitro* was 0.1–0.5 mW s⁻¹. The stimulus was repeated with a frequency of once a minute.

We found that careful adjustment of the light stimulus slope could induce oscillations lasting up to 30 s *in vitro* and *in vivo*. The power of activity typically decremented during the course of the stimulus probably owing to a combination of adaptive phenomena, including synaptic depression, spike after-hyperpolarization, and intrinsic desensitization of ChR2. Square light pulses lasted 5 ms at the constant power of 2 mW.

For restricted photostimulation of a circular area of ~ 90 μ m in diameter we closed the field diaphragm of the BX51 to its minimal aperture. Microscope translation was controlled by custom routines written in Igor Pro (Wavemetrics) via the Nidaq Card and a Newport ESP600 controller. The spatial extent of neuronal recruitment by this circular photostimulus was determined as follows: we recorded from ChR2-expressing layer 2/3 pyramidal cells in the loose-patch or cell-attached configuration (Supplementary Fig. 6), and recorded the firing rate of the pyramidal cell as a function of the distance of its soma from the centre of the photostimulated area (the photostimulus was moved tangentially along the pyramidal cell layer). The firing rate of the pyramidal cells fell to $6 \pm 3\%$ ($n = 5$) of its maximal firing rate 120 μ m from the centre of the photostimulated area. Thus, the circular photostimulus recruited pyramidal cells within a restricted area of approximately one barrel column in diameter (Supplementary Fig. 6). For experiments at the edge of barrel cortex, the most lateral barrel observed under the light microscope was centred and stimulation locations were at 200 μ m intervals on either side of the layer 2/3 cell recorded in that barrel column.

Excitatory and inhibitory charges. Excitatory and inhibitory currents were isolated by voltage clamping the neuron at the reversal potential for synaptic inhibition and excitation respectively. The current was integrated over a 1 s period from the onset of the light ramp. For oscillations initiated *in vitro* the net excitatory charge averaged (in pC): L2/3, 87 ± 7 , $n = 58$; L4, 4 ± 1 , $n = 16$; L5, 107 ± 14 , $n = 34$; L6, 4 ± 1 , $n = 15$. The excitatory power between 20–60 Hz averaged (in $10^3 \text{ pA}^2 \text{Hz}^{-1}$): L2/3, 1.7 ± 0.6 , $n = 46$; L4, 0.014 ± 0.004 , $n = 15$; L5, 2.5 ± 0.9 , $n = 20$; L6, 0.03 ± 0.02 , $n = 14$. The net inhibitory charge averaged (in pC): L2/3, 605 ± 50 , $n = 53$; L4, 16 ± 4 , $n = 16$; L5, 540 ± 70 , $n = 32$; L6, 10 ± 2 , $n = 13$. The inhibitory power between 20–60 Hz averaged (in $10^4 \text{ pA}^2 \text{Hz}^{-1}$): L2/3, 4 ± 1 ; L4, 0.03 ± 0.01 ; L5, 4 ± 1 ; L6, 0.03 ± 0.02 . These data

are averaged across all simultaneous dual and quadruple recordings (Fig. 2b). For simultaneous recordings of layer 5A and layer 5B pyramidal cells, the excitatory charge averaged (in pC): L5A, 58 ± 10 ; L5B, 104 ± 58 , $n = 11$. The excitatory power between 20–60 Hz averaged (in $10^3 \text{ pA}^2 \text{ Hz}^{-1}$): L5A, 2.2 ± 0.9 ; L5B, 6 ± 1 , $n = 11$. The inhibitory charge averaged (in pC): L5A, 230 ± 40 ; L5B, 360 ± 80 , $n = 11$. The inhibitory power between 20–60 Hz averaged (in $10^4 \text{ pA}^2 \text{ Hz}^{-1}$): L5A, 2.0 ± 0.9 ; L5B, 8 ± 2 , $n = 11$ (Supplementary Fig. 5).

Data acquisition and analysis. *In vitro* data were recorded with Multiclamp 700B amplifiers (Axon instruments) filtered at 2 kHz and digitized with a Nidaq Card at 10 kHz. Data *in vivo* were recorded with Axopatch 200A (Axon instruments) filtered at 2 kHz and digitized with a Nidaq Card at 10 kHz. For multichannel recording an AM systems 16-channel model 3500 amplifier was used, filtered at 0.3–5,000 Hz and digitized at 30 kHz.

All data acquisition, analogue output control and analysis were performed by custom routines written in Igor Pro (Wavemetrics). Average values are expressed as means \pm s.e.m. The student *t*-test, paired *t*-test, one-way ANOVA and Kolmogorov–Smirnov tests were used for statistical comparisons, as indicated in the results. Drugs used were NBQX, CPP and SR95531 (gabazine) (Tocris Cookson).

To measure the speed of propagation of the oscillation we simultaneously recorded from pairs of layer 2/3 cells either immediately next to each other, or 300–400 μm apart, and focally stimulated with light ramps as described above. We then computed the cross-correlation of their rhythmic excitatory or inhibitory inputs and divided the lag of the peak of the cross-correlogram by their inter-somatic distance. Neighbouring cells had a lag of $0.26 \pm 0.15 \text{ ms}$ ($n = 3$) whereas separated cells had a lag of $1.7 \pm 0.3 \text{ ms}$ ($n = 6$, $P = 0.004$).

Bypassing axons expressing ChR2 do not contribute to oscillatory activity. Photoinitiated gamma activity necessitated an intact somatodendritic compartment of ChR2-expressing pyramidal cells, as light-ramp photostimulation of cortical areas containing only ChR2-expressing axons (for example, layer 5; Supplementary Fig. 6), although transiently inducing some transmitter release (only $5 \pm 2\%$ of the charge as compared to stimulation on layer 2/3 in the same slices), did not lead to gamma oscillations. Thus, whereas strong light pulses can directly evoke release from ChR2-expressing axons^{24,25}, at the intensities used to evoke gamma oscillations in this study, rhythmic release from directly stimulated axons was negligible.

Replay of synaptic currents. Layer 2/3 and Layer 5 pyramidal cells were patched with two pipettes at the soma in the current clamp configuration, one to impose an inhibitory conductance, the other to inject an excitatory current. The inhibitory conductance waveform had the amplitude and time course of an inhibitory conductance recorded at the soma of either a layer 2/3 or a layer 5 pyramidal cell during photoinduced oscillations. The waveforms were taken from pairs of simultaneously recorded layer 2/3 or layer 5 cells where one cell was held at EPSC reversal and the other at IPSC reversal to preserve the relative temporal relationship of the two conductances. Additionally, their excitation and inhibition ratio approximated the mean measured from our sample of simultaneously recorded layer 2/3 and layer 5 cells.

To impose the inhibitory conductance (dynamic clamp), the external command of the amplifier connected to one of the pipettes was controlled such as to inject a current that was, at any time point, equal to the conductance times the difference between the membrane potential of the neuron and the reversal potential for inhibition, set at -60 mV . The operation was performed by a custom-made analogue circuit (5 MHz bandwidth) receiving an input from the amplifier for the membrane potential of the neuron, an analogue input for the conductance waveform, and sending an output to the external command of the amplifier to control the current injected into the neuron.

The excitatory input was simulated by directly injecting, through the other pipette, excitatory current waveforms recorded during photoinduced oscillations at the soma of either a layer 2/3 or a layer 5 pyramidal cell voltage clamped at -70 mV .

In each experiment a square depolarizing current step was first injected alone to elicit baseline firing at 3–9 Hz (Fig. 5c, left), this current step was then delivered again together with the excitatory and inhibitory waveforms (Fig. 5c, middle and right).

We tested the impact of excitatory and inhibitory waveforms on spike rate modulation by re-injecting these waveforms in the soma despite the fact that excitatory and inhibitory synaptic inputs are distributed along the somatodendritic axis pyramidal cells. We reasoned that because in pyramidal cells the axon initial segment, where action potentials are initiated^{35,36,46}, originates from the soma, the waveform that matters in terms of spike rate modulation is the one recorded at the soma. Simply stated, injecting a waveform in the soma should reproduce the original somatic membrane potential trajectory as long as what is injected in the soma is what is recorded at the soma. We have ascertained the accuracy of this hypothesis using a simple ball-stick simulation of a neuron implemented in the NEURON environment⁴⁷. We compared the somatic membrane potential fluctuation of the model neuron in response to the following two conditions: (1) a simulated excitatory synaptic conductance into the dendrite; (2) somatic injection of the excitatory waveform obtained under somatic voltage clamp in response to the same dendritic conductance injection. Consistent with imperfect space clamp, the conductance obtained under somatic voltage clamp was (relative to the conductance at its site of origin in the dendrites) diminished in amplitude, temporally filtered, and had an apparent reversal potential above 0 mV; that is, above the reversal potential of the excitatory conductance at its site of origin. However, re-injecting this waveform into the soma generated a somatic membrane potential trajectory that was identical to that obtained in response to the dendritic conductance. Thus, our somatic replay of somatically recorded waveforms probably closely reproduces the somatic membrane potential fluctuations experienced by pyramidal cells in response to spatially distributed synaptic inputs.

45. Niell, C. M. & Stryker, M. P. Highly selective receptive fields in mouse visual cortex. *J. Neurosci.* **28**, 7520–7536 (2008).

46. Palmer, L. M. & Stuart, G. J. Site of action potential initiation in layer 5 pyramidal neurons. *J. Neurosci.* **26**, 1854–1863 (2006).

47. Carnevale, N. T. & Hines, M. L. *The NEURON Book* (Cambridge Univ. Press, 2006).